



ARTICLE

Identification and characterization of a series of novel HCN channel inhibitors

Shu-jun Chen¹, Yao Xu¹, Ye-mei Liang¹, Ying Cao¹, Jin-yan Lv¹, Jian-xin Pang¹ and Ping-zheng Zhou¹

Hyperpolarization-activated cyclic nucleotide-gated (HCN) channels play a critical role in controlling pacemaker activity in both heart and nervous system. Developing HCN channel inhibitors has been proposed to be an important strategy for the treatment of pain, heart failure, arrhythmias, and epilepsy. One HCN channel inhibitor, ivabradine, has been clinically approved for the treatment of angina pectoris and heart failure. In this study, we designed and synthesized eight alkanol amine derivatives, and assessed their effects on HCN channels expressed in COS7 cells using a whole-cell patch clamp method. Among them, compound **4e** displayed the most potent inhibitory activity with an IC_{50} of $2.9 \pm 1.2 \mu\text{M}$ at -120 mV on HCN2 channel expressed in COS7 cells. Further analysis revealed that application of compound **4e** ($10 \mu\text{M}$) caused a slowing of activation and a hyperpolarizing shift ($\Delta V_{1/2} = -30.2 \pm 2.9 \text{ mV}$, $n = 5$) in the voltage dependence of HCN2 channel activation. The inhibitory effect of compound **4e** on HCN1 and HCN4 channel expressed in COS7 cells was less potent with IC_{50} of 17.2 ± 1.3 and $7.3 \pm 1.2 \mu\text{M}$, respectively. Besides, we showed that application of compound **4e** ($10 \mu\text{M}$) inhibited I_h and action potential firing in acutely dissociated mouse small dorsal root ganglion neurons. Our study provides a new strategy for the design and development of potent HCN channel inhibitors.

Keywords: HCN channel; whole-cell patch clamp; pain; heart failure; structure-activity relationship

Acta Pharmacologica Sinica (2019) 40:746–754; <https://doi.org/10.1038/s41401-018-0162-z>

INTRODUCTION

Hyperpolarization-activated cyclic nucleotide-gated (HCN) channels are activated by membrane hyperpolarization and conduct mixed Na^+/K^+ currents, thus contributing to pacemaker depolarization, which generates rhythmic activity in sinoatrial node cells and spontaneously active neurons [1–5]. One notable characteristic of HCN channels is that they are dually activated by voltage hyperpolarization and intracellular cyclic adenosine monophosphate (cAMP) [6–10]. To date, four mammalian HCN isoforms (HCN 1–4) have been identified, each with distinct biophysical, modulatory properties, and diverse tissue distributions [4, 5, 11, 12]. HCN4 is preferentially expressed in the sinoatrial node cells of mammals [13, 14]. Loss-of-function mutations of the HCN4 gene have been identified as responsible for several heart channelopathies [15–18]. All HCN isoforms are widely expressed in the central and peripheral nervous system. Dysfunctional HCN channels in the nervous system are involved in numerous pathologic processes such as pain, epilepsy, autism spectrum disorder, schizophrenia, and mood disorders [5, 19]. HCN channels have been proposed as a novel target for pharmacological intervention for angina, heart failure, pain, and epilepsy [20].

Two classes of HCN channel inhibitors have been identified and broadly studied, including “bradine” compounds (zatebradine, cilobradine, and ivabradine) and ZD7288 (chemical structures in Fig. 1). Among all “bradine” compounds, ivabradine is the only one that is clinically approved for the treatment

of angina pectoris and heart failure [20–22]. ZD7288 is another HCN channel blocker, which is structurally unrelated to “bradine” compounds and is broadly used as a tool to study the biophysical and physiological properties of HCN channels [23, 24]. Both ivabradine and ZD7288 block all HCN isoforms to a similar extent, and they are thought to be pore blockers with similar action sites on HCN channels [24–27]. Recently, structural modifications of the nonselective inhibitor zatebradine generated several new inhibitors (EC18, MEL55A and MEL57A), which show subtype selectivity towards different HCN subtypes [28, 29]. The discovery of inhibitors with novel structural backbones and subtype selectivities could be beneficial for both the biophysical and pharmacological study of HCN channels.

During our initial efforts to identify novel HCN channel inhibitors, we serendipitously discovered that compound **4a** inhibited the HCN2 channel significantly. Furthermore, we designed and synthesized a series of novel alkanol amine compounds based on compound **4a** and evaluated their ability to inhibit the HCN channels. The most potent compound, **4e**, blocked the HCN2 current with an IC_{50} of $2.9 \pm 1.2 \mu\text{M}$ at -120 mV . In addition to blocking channel conductance, **4e** caused a slowing of activation and a hyperpolarizing shift of the voltage dependence of HCN2 channel activation. Moreover, we found that **4e** blocked I_h in small dorsal root ganglion (DRG) neurons and inhibited its action potential firing. Our study may provide a new structural backbone for the development of future HCN channel inhibitors.

¹Guangdong Provincial Key Laboratory of New Drug Screening, School of Pharmaceutical Sciences, Southern Medical University, Guangzhou 510515, China

Correspondence: Ping-zheng Zhou (zhoupingzheng@126.com)

These authors contributed equally: Shu-jun Chen and Yao Xu

Received: 2 February 2018 Accepted: 13 August 2018

Published online: 12 October 2018

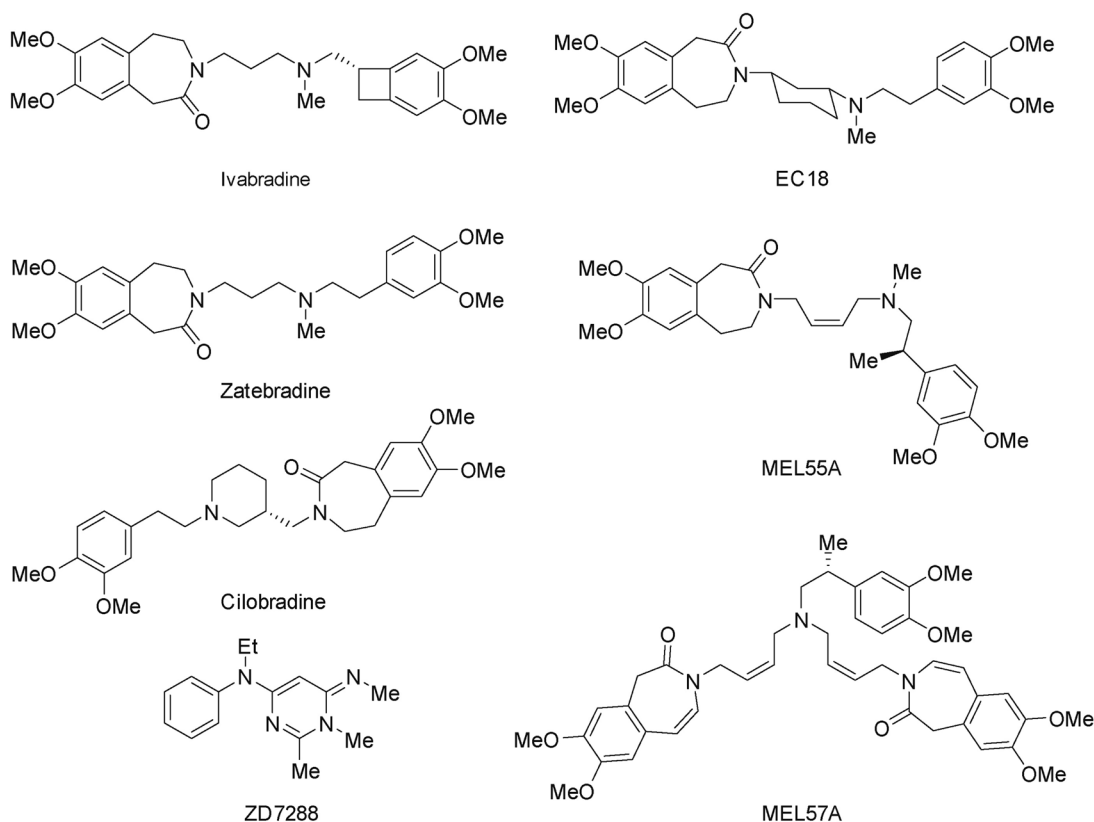
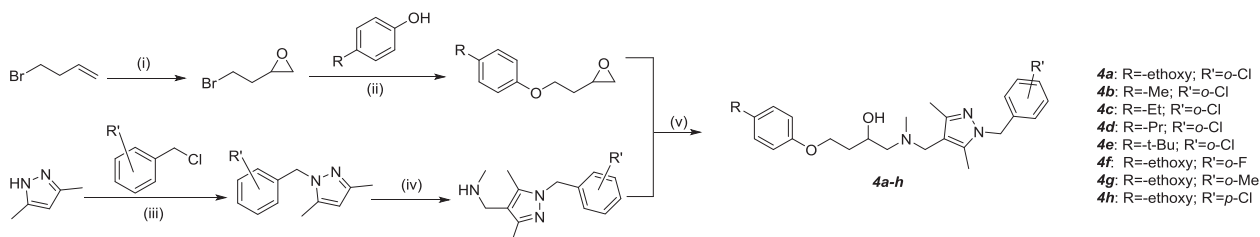


Fig. 1 Structures of known HCN channel inhibitors



Scheme 1 Synthesis of alkanol amine derivatives. Reagents and conditions. (i) mCPBA, CH_2Cl_2 , rt, 24 h. (ii) K_2CO_3 , acetone, Rf, 16 h. (iii) 3,5-dimethyl-1H-pyrazole, KOH, DMSO, 80 °C, 1.5 h; then benzyl chloride, rt, 2 h. (iv) CH_3NH_2 , (CHO) $_n$, EtOH, Rf, 16 h. (v) EtOH, Rf, 24 h

MATERIALS AND METHODS

Chemistry

All of the compounds were synthesized according to Scheme 1; 4-bromobut-1-ene and mCPBA were used to synthesize 2-(2-bromoethyl)oxirane. The 2-(2-phenoxyethyl)oxirane was synthesized by substituted phenol derivatives and 2-(2-bromoethyl)oxirane. Connection with 3,5-dimethylpyrazole and substituted benzyl chloride in weak base resulted in the 1-benzyl-3,5-dimethyl-1H-pyrazole derivatives. The corresponding secondary amine compounds were prepared with paraformaldehyde and methylamine hydrochloride in ethanol through the Mannich reaction. 2-(2-phenoxyethyl)oxirane and a secondary amine were refluxed in ethanol to give the targeted products (**4a–h**).

Cell culture and transfection

COS7 cells were cultured in Dulbecco's modified Eagle's medium (DMEM) (Life Technologies, USA) containing 10% fetal bovine serum (FBS) and maintained at 37 °C with a 5% CO_2 atmosphere.

The open reading frames of human HCN1 (NM_021072.3), mouse HCN2 (NM_008226.2), and mouse HCN4 (NM_001081192.1) were synthesized, sequenced, and further cloned into pEGFP-N1 vectors.

To express the HCN channels, COS7 cells were cultured in a six-well plate, maintained overnight, and then transiently transfected with 1.5 μg plasmid DNA (HCN1, HCN2, or HCN4) using Lipofectamine 2000 reagent (Life Technologies) according to the manufacturer's instructions. After 24–48 h, cells were split and redistributed onto coverslips coated with 0.1 mg/mL poly-L-lysine (Sigma-Aldrich, USA) for the following electrophysiological experiments.

Acute dissociation of DRG neurons

DRG neurons were isolated from 4–6-week-old wild-type C57BL/6 male mice. In brief, all mice were killed by cervical dislocation followed by decapitation, and DRG neurons were dissected from the entire length of the spinal column and placed directly into cooled phosphate-buffered saline as a cleaning step. The DRG neurons were digested with DMEM containing 2 mg/mL collagenase type IA (Sigma-Aldrich, USA) and 0.5 mg/mL trypsin (Solarbio, USA) for 40 min at 37 °C. After terminating the enzymatic treatment by FBS, DRG neurons were centrifuged at 1000 r/min for 5 min, and the supernatant was discarded and resuspended in 1 mL DMEM supplemented with 10% FBS, 100 U/mL penicillin, and 100 mg/mL streptomycin. Cells were plated onto coverslips coated

with 0.1 mg/mL poly-L-lysine and kept at 37 °C in an incubator with 5% CO₂. All electrophysiological recordings were made within 4–72 h after dissociation.

Whole-cell patch clamp recording

Whole-cell HCN channel currents were recorded using an Axopatch-700B amplifier interfaced to a Digidata 1550B data acquisition system using the pClamp 10.6 software (Molecular Devices, USA). Recording pipettes were pulled from borosilicate glass capillaries using a P-97 horizontal micropipette puller (Sutter Instrument, USA) and had an average resistance of 2–5 MΩ. The data were filtered at 2 kHz and digitized at 20 kHz. The pipette electrode for the COS7 cells contained (in mM): 140 KCl, 1 MgCl₂, 5 EGTA, and 10 HEPES (pH 7.4 with KOH). The extracellular solution contained (in mM): 140 NaCl, 5 KCl, 2 CaCl₂, 1 MgCl₂, 10 glucose, and 10 HEPES (pH 7.4 with NaOH). Patch pipettes for the DRG neurons were filled with an internal solution containing (in mM): 140 K-aspartate, 5 EGTA, 2 MgCl₂, 10 HEPES, 0.5 NaGTP and 2 MgATP (pH 7.4 with KOH). All whole-cell recordings were completed at room temperature (25 ± 2 °C).

Electrophysiological data were processed using Clampfit 10.6 (Molecular Devices, USA) and then analyzed in GraphPad Prism 5 (GraphPad Software, USA). Voltage-dependent activation curves were fitted with the Boltzmann equation $G = G_{\min} + (G_{\max} - G_{\min}) / (1 + \exp((V - V_{1/2})/S))$, where G_{\max} is the maximum conductance, G_{\min} is the minimum conductance, $V_{1/2}$ is the voltage for half-activation potential, and S is the slope factor. The time constants for activation (τ_{act}) or deactivation (τ_{deact}) were obtained by fitting the HCN current tracings at -120 mV with a monoexponential function using Clampfit 10.6. Dose-response curves were obtained by fitting to the Hill equation, $E = E_{\min} + (E_{\max} - E_{\min}) / (1 + 10^{-(\text{Log}(I_{50} - C)^n))}$, where $E = I_{\text{drug}}/I_{\text{control}}$, E_{\max} and E_{\min} are the maximally and minimally inhibited responses, respectively, I_{50} corresponds to the concentration that provokes a response halfway between E_{\max} and E_{\min} , C corresponds to the drug concentration, and n is the Hill coefficient. Data are expressed as the mean ± SEM. Statistical analysis was conducted using Student's *t* test or one-way analysis of variance where appropriate, and results were considered significant when $P < 0.05$.

Application of compounds

All compounds were dissolved in dimethyl sulfoxide to prepare a stock solution with a concentration of 100 mM, from which the appropriate volumes were added to the extracellular solution to obtain the desired concentrations and applied to the cells through perfusion.

RESULTS

Synthesis of alkanol amine derivatives

4a: Yield 84%; ¹H NMR (400 MHz, CDCl₃) δ 7.37 (d, $J = 8.0$ Hz, 1 H), 7.23–7.11 (m, 2 H), 6.84 (d, $J = 1.6$ Hz, 4 H), 6.52–6.48 (m, 1 H), 5.32 (s, 2 H), 4.13–3.91 (m, 5 H), 3.53–3.25 (m, 2 H), 2.48–2.31 (m, 2 H), 2.27 (s, 3 H), 2.23 (s, 3 H), 2.12 (s, 3 H), 1.93–1.78 (m, 2 H), 1.42–1.37 (m, 3 H). ¹³C NMR (101 MHz, CDCl₃) δ 153.08, 152.88, 147.83, 134.98, 131.72, 129.21, 128.57, 127.38, 127.24, 115.42, 115.40, 115.35, 77.27, 66.62, 65.28, 64.19, 63.95, 62.81, 51.35, 50.08, 41.49, 34.61, 32.62, 14.88, 12.13, 9.65. ESI-MS (Electrospray ionization-mass spectrometry): m/z calcd for C₂₆H₃₄ClN₃O₃ (M + H⁺) 471.2, found 471.4.

4b: Yield 75%; ¹H NMR (400 MHz, CDCl₃) δ 7.38 (d, $J = 8.0$ Hz, 1 H), 7.25–7.13 (m, 2 H), 7.09 (d, $J = 7.6$ Hz, 2 H), 6.83 (d, $J = 8.4$ Hz, 2 H), 6.52 (d, $J = 7.6$ Hz, 1 H), 5.33 (s, 2 H), 4.15–4.11 (m, 2 H), 3.99 (s, 1 H), 3.56–3.50 (m, 1 H), 3.36–3.31 (m, 1 H), 2.53–2.48 (m, 1 H), 2.42–2.37 (m, 1 H), 2.32–2.24 (m, 9 H), 2.14 (s, 3 H), 1.98–1.79 (m, 2 H). ¹³C NMR (101 MHz, CDCl₃) δ 156.64, 147.82, 139.60, 138.59, 138.32, 137.91, 129.80, 129.80, 129.20, 128.57, 127.36, 127.23, 114.33, 77.16, 64.70, 64.27, 62.82, 51.35, 50.71, 50.04, 41.52, 34.53,

20.38, 12.06, 9.59. ESI-MS: m/z calcd for C₂₅H₃₂ClN₃O₂ (M + H⁺) 441.2, found 441.4.

4c: Yield 79%; ¹H NMR (400 MHz, CDCl₃) δ 7.38 (d, $J = 7.6$ Hz, 1 H), 7.22–7.16 (m, 2 H), 7.10 (d, $J = 8.0$ Hz, 2 H), 6.85 (d, $J = 8.4$ Hz, 2 H), 6.53 (d, $J = 7.6$ Hz, 1 H), 5.33 (s, 2 H), 4.14 (t, $J = 7.6$ Hz, 2 H), 4.03 (s, 1 H), 3.58 (s, 1 H), 3.39 (s, 1 H), 2.72–2.54 (m, 3 H), 2.45–2.41 (m, 1 H), 2.28 (s, 6 H), 2.16 (s, 3 H), 1.97–1.83 (m, 2 H), 1.23 (t, $J = 7.6$ Hz, 3 H). ¹³C NMR (101 MHz, CDCl₃) δ 156.79, 147.83, 141.44, 136.41, 134.96, 131.72, 129.21, 128.63, 128.63, 127.38, 127.23, 114.34, 114.34, 98.22, 64.67, 64.25, 62.82, 51.35, 50.76, 50.06, 41.50, 34.55, 27.90, 15.81, 12.10, 9.63. ESI-MS: m/z calcd for C₂₆H₃₄ClN₃O₂ (M + H⁺) 455.3, found 455.4.

4d: Yield 82%; ¹H NMR (400 MHz, CDCl₃) δ 7.38 (d, $J = 7.6$ Hz, 1 H), 7.23–7.13 (m, 2 H), 7.10 (d, $J = 8.4$ Hz, 2 H), 6.84 (d, $J = 8.4$ Hz, 2 H), 6.52 (d, $J = 7.6$ Hz, 1 H), 5.33 (s, 2 H), 4.16–4.11 (m, 2 H), 4.02–3.94 (m, 1 H), 3.56–3.50 (m, 1 H), 3.36–3.30 (m, 1 H), 2.54 (t, $J = 7.6$ Hz, 2 H), 2.49–2.45 (m, 1 H), 2.41–2.35 (m, 1 H), 2.28–2.25 (m, 5 H), 2.14 (s, 3 H), 1.97–1.77 (m, 2 H), 1.66–1.59 (m, 2 H), 1.29–1.24 (m, 1 H), 0.95 (t, $J = 7.3$ Hz, 3 H). ¹³C NMR (101 MHz, CDCl₃) δ 156.84, 147.81, 138.51, 135.04, 134.79, 131.71, 129.23, 129.23, 129.23, 129.20, 128.55, 127.37, 127.23, 114.24, 114.17, 64.67, 64.25, 62.85, 51.37, 50.06, 41.52, 37.09, 34.58, 24.71, 13.72, 12.12, 9.60. ESI-MS: m/z calcd for C₂₇H₃₆ClN₃O₂ (M + H⁺) 469.3, found 469.3.

4e: Yield 77%; ¹H NMR (400 MHz, CDCl₃) δ 7.39 (d, $J = 6.8$ Hz, 1 H), 7.31 (d, $J = 8.4$ Hz, 2 H), 7.22–7.15 (m, 2 H), 6.86 (d, $J = 8.8$ Hz, 2 H), 6.52 (d, $J = 7.6$ Hz, 1 H), 5.33 (s, 2 H), 4.15 (t, $J = 5.2$ Hz, 2 H), 4.01 (s, 1 H), 3.58–3.52 (m, 1 H), 3.40–3.34 (m, 1 H), 2.54 (s, 1 H), 2.42 (s, 1 H), 2.28 (s, 6 H), 2.15 (s, 3 H), 1.95–1.83 (m, 2 H), 1.32 (s, 9 H). ¹³C NMR (101 MHz, CDCl₃) δ 156.53, 147.80, 143.28, 138.46, 135.07, 131.70, 129.19, 128.54, 127.37, 127.23, 126.13, 126.13, 113.91, 113.91, 64.63, 64.26, 62.88, 51.39, 50.06, 41.54, 34.58, 33.99, 31.47, 31.47, 31.47, 12.12, 9.59. ESI-MS: m/z calcd for C₂₈H₃₈ClN₃O₂ (M + H⁺) 483.2, found 483.3.

4f: Yield 82%; ¹H NMR (400 MHz, CDCl₃) δ 7.27–7.22 (m, 1 H), 7.11–7.01 (m, 2 H), 6.85 (s, 5 H), 5.29 (s, 2 H), 4.10 (t, $J = 6.4$ Hz, 2 H), 4.00 (q, $J = 7.2$ Hz, 3 H), 3.56–3.50 (m, 1 H), 3.36–3.30 (m, 1 H), 2.52 (s, 1 H), 2.42–2.36 (m, 1 H), 2.26 (s, 6 H), 2.18 (s, 3 H), 1.91–1.80 (m, 2 H), 1.41 (t, $J = 7.0$ Hz, 3 H). ¹³C NMR (101 MHz, CDCl₃) δ 153.04, 152.93, 147.57, 138.10, 129.07, 128.49, 124.48, 124.34, 115.39, 115.33, 115.33, 115.19, 114.98, 113.36, 65.33, 64.25, 63.92, 62.93, 51.40, 46.11, 46.06, 41.53, 34.61, 14.89, 12.09, 9.51. ESI-MS: m/z calcd for C₂₆H₃₄FN₃O₃ (M + H⁺) 455.3, found 455.5.

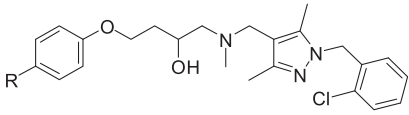
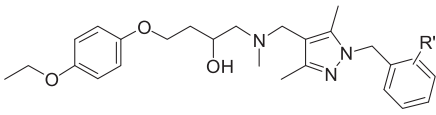
4g: Yield 69%; ¹H NMR (400 MHz, CDCl₃) δ 7.17 (d, $J = 8.4$ Hz, 2 H), 7.12–7.08 (m, 1 H), 6.85 (s, 4 H), 6.45 (d, $J = 7.2$ Hz, 1 H), 5.21 (s, 2 H), 4.14–4.08 (m, 2 H), 4.00 (q, $J = 7.2$ Hz, 3 H), 3.56–3.50 (m, 1 H), 3.36–3.30 (m, 1 H), 2.55–2.47 (m, 1 H), 2.40 (s, 1 H), 2.35 (s, 3 H), 2.27 (s, 6 H), 2.12 (s, 3 H), 1.97–1.80 (m, 2 H), 1.41 (t, $J = 7.2$ Hz, 3 H). ¹³C NMR (101 MHz, CDCl₃) δ 153.05, 152.97, 147.34, 138.35, 135.41, 134.61, 130.08, 127.19, 126.34, 125.67, 115.41, 115.41, 115.35, 115.35, 65.34, 64.23, 63.95, 62.87, 51.41, 50.71, 50.68, 41.50, 34.62, 19.00, 14.89, 12.09, 9.70. ESI-MS: m/z calcd for C₂₇H₃₇N₃O₃ (M + H⁺) 451.3, found 451.6.

4h: Yield 68%; ¹H NMR (400 MHz, CDCl₃) δ 7.30 (s, 1 H), 7.28 (s, 1 H), 7.00 (d, $J = 8.0$ Hz, 2 H), 6.85 (s, 4 H), 5.20 (s, 2 H), 4.12–4.08 (m, 2 H), 4.00 (q, $J = 6.8$ Hz, 3 H), 3.56–3.50 (m, 1 H), 3.36–3.30 (m, 1 H), 2.55–2.46 (m, 1 H), 2.41–2.35 (m, 1 H), 2.26 (s, 6 H), 2.14 (s, 3 H), 1.97–1.75 (m, 2 H), 1.41 (t, $J = 6.8$ Hz, 3 H). ¹³C NMR (101 MHz, CDCl₃) δ 153.07, 152.90, 147.51, 135.73, 133.29, 128.84, 128.84, 127.84, 127.84, 115.39, 115.39, 115.35, 115.35, 77.15, 65.28, 64.20, 63.95, 62.89, 52.06, 51.34, 41.49, 34.60, 14.89, 12.07, 9.77. ESI-MS: m/z calcd for C₂₆H₃₄ClN₃O₃ (M + H⁺) 471.2, found 471.3.

Identification of a series of HCN channel blockers

We first examined the effects of the synthesized compounds on the HCN2 channel, which was heterologously expressed in COS7 cells. The HCN2 current was elicited by a hyperpolarizing potential of -120 mV, and the effects on the amplitude of the inward current (I_{I_0}) were analyzed. The lead compound **4a** (10 μM)

Table 1 Effects of alkanol amine compounds on HCN2 currents in COS7 cells

					
Compound	R	I/I_0 ^[a]	Compound	R'	I/I_0
4a	-ethoxy	0.56 ± 0.02	4f	<i>o</i> -F	0.28 ± 0.01
4b	-Me	0.53 ± 0.04	4g	<i>o</i> -Me	0.62 ± 0.05
4c	-Et	0.43 ± 0.05	4h	<i>p</i> -Cl	0.57 ± 0.05
4d	-Pr	0.37 ± 0.02			
4e	- <i>t</i> -Bu	0.26 ± 0.01			

^a I_0 is the amplitude of inward HCN2 currents at -120 mV in the control condition, whereas I is the amplitude of inward HCN2 currents in the presence of the corresponding compound at 10 μ M. Each compound was tested on at least at two different days and in 4–8 cells.

blocked the HCN2 current at -120 mV to 56% ($n = 14$) (Table 1), which was a stronger inhibitory effect on the HCN2 channel compared with ZD7288 ($n = 4$; $P < 0.01$) (Supplementary Fig. 1).

Comparing the compounds from **4b** to **4e** showed a substitution of the para- position on the R group with a series of extended carbon chains, which markedly enhanced the inhibitory efficacy. The inhibitory effect significantly increased in particular with the tert-butyl group in **4e**, which indicated the large hindrance substitution was helpful for the activity (Table 1).

Replacement of the *o*Cl on the R' group with an electron-withdrawing group (**4f**) also strongly augmented the compound's inhibitory effect on the HCN2 channel, whereas adding a weak electron-donating group (**4g**) had no significant effect on its inhibitory action. Moreover, substitution of the *o*Cl with *p*Cl (**4h**) also had no significant influence on the compound's inhibitory action (Table 1).

Electrophysiological properties of **4e** blockage on HCN2 channel We selected the most potent inhibitor, **4e**, for further characterization of its inhibitory properties on HCN channels. We first tested the inhibitory effect of **4e** on the HCN2 channel under a testing voltage of -120 mV and used different concentrations to evaluate the IC_{50} . Fig. 2a showed the typical HCN2 current traces in the absence or presence of 10 μ M **4e**. Dose-response curves showed that the IC_{50} of **4e** on the HCN2 channel was $2.9 \pm 1.2 \mu$ M (Fig. 2b), which was similar to the reported IC_{50} of ivabradine on heterologously expressed HCN channels [30]. Then, we elicited HCN2 current at different voltages from -50 to -140 mV. The data showed that 10 μ M **4e** markedly decreased the HCN2 current in all tested voltages, (Fig. 2c, d) and the normalized I - V relationship that was determined for multiple COS7 cells ($n = 5$) was plotted in Fig. 2e. The voltage dependence of the current activation normalized to G_{max} for each cell was plotted in Fig. 2f, demonstrating that the voltage-dependent activation was drastically shifted in a more hyperpolarized direction after the treatment with 10 μ M **4e** ($\Delta V_{1/2} = -30.2 \pm 2.9$ mV, $n = 5$) (Table 2). In addition, **4e** slowed down the activation speed dramatically at -120 mV, but it had no effect on the deactivation process that was measured at +50 mV after a test pulse to -130 mV (Table 2).

Subtype selectivity of **4e** on HCN channels

To investigate the selectivity of **4e** toward other HCN subtypes, compound **4e** was further tested on the HCN1 and HCN4 channels. Representative current tracings from COS7 cells expressing HCN1 and HCN4 before and after the application of 10 μ M **4e** are shown in Fig. 3a, b. In total, 10 μ M **4e** blocked both HCN1 and HCN4 but to a less potent extent compared with its effect on HCN2, whose $I/I_0 = 0.65 \pm 0.01$ ($n = 15$) for HCN1 and $I/I_0 = 0.56 \pm 0.04$ ($n = 9$) for HCN4 (Fig. 3c). Moreover, dose-response curves determined that the IC_{50} of **4e** was $17.2 \pm 1.3 \mu$ M for HCN1 and $7.3 \pm 1.2 \mu$ M for HCN4, respectively (Fig. 3d, e). The effects of **4e** on HCN1 and HCN4 under different voltages were further investigated. Similarly, to its effect of **4e** on the HCN2 channel, it also reduced the HCN1 and HCN4 currents in all tested voltages (Fig. 4c, d). Moreover, 10 μ M **4e** induced hyperpolarizing shifts on the voltage-dependent activation curves of the HCN1 and HCN4 channels ($\Delta V_{1/2} = -30.4 \pm 3.7$ mV, $n = 4$ for HCN1; $\Delta V_{1/2} = -20.3 \pm 3.4$ mV, $n = 4$ for HCN4) (Fig. 4e, f). In addition, we noted that the rate constants for activation, which were obtained from each isoform at -120 mV, were significantly increased in the presence of 10 μ M **4e**, whereas there were no significant differences in deactivation rate, similar to what was described for the HCN2 channel (Table 2).

4e inhibited HCN channels in a non-use-dependent manner

Consistent with previous research, ZD7288 was an apparent non-use-dependent inhibitor of the HCN1 channel [31] (Supplementary Fig. 2). Then, we examined whether **4e** was a use-dependent inhibitor of HCN channels with the same protocol. In all tested isoforms of the HCN channels, application of 10 μ M **4e** led to a reduction of HCN-mediated current when cells were held at -30 mV, indicating that **4e** could inhibit HCN channels regardless of channel conformation (Fig. 5). Applying 10 μ M **4e** without activation of the HCN1 or HCN4 channel initially resulted in a similar extent of inhibition compared to the condition of when HCN1 and HCN4 were activated every 15 s (Fig. 5a, c). For the HCN2 channel, **4e** initially resulted in an inhibition by $39\% \pm 5\%$ ($n = 4$) of the HCN2 current, and the inhibition gradually reached the stable state after the channel activation was resumed, resulting in a final inhibition of $69\% \pm$

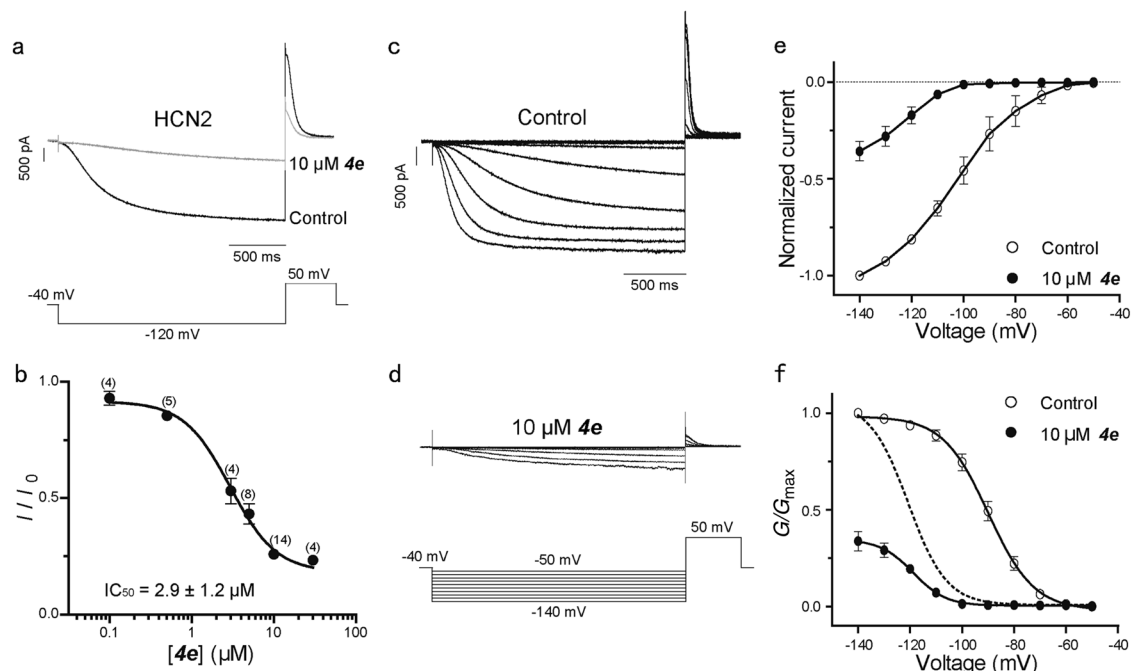


Fig. 2 Electrophysiological properties of **4e** blocking HCN2 current. **a** Typical HCN2 current traces in the absence or presence of **4e** ($10\ \mu\text{M}$). HCN2 current was elicited by a 2 s hyperpolarizing step at $-120\ \text{mV}$ from a holding potential of $-40\ \text{mV}$, tail current was measured at $+50\ \text{mV}$ and the protocol was applied every 15 s until achieving stable inhibition. **b** Dose-response relationship of **4e** on the HCN2 channel recorded at $-120\ \text{mV}$ at different concentrations (0.1, 0.5, 3, 5, 10, or $30\ \mu\text{M}$, as indicated). **c**, **d** Representative traces of HCN2 current in the control condition **c** or with the perfusion of $10\ \mu\text{M}$ **4e** **d**. HCN2 current was recorded by a series of hyperpolarizing steps ranging from $-50\ \text{mV}$ to $-140\ \text{mV}$ in $-10\ \text{mV}$ decrements from a holding potential of $-40\ \text{mV}$. Voltage was then returned to $+50\ \text{mV}$ to measure the tail current. **e** Normalized I - V relationships recorded before and after the application of $10\ \mu\text{M}$ **4e** on HCN2 channel. **f** Normalized voltage-dependent activation curves of the HCN2 channel before and after treatment with $10\ \mu\text{M}$ **4e**. The dotted curve represented data normalized to its own peak amplitude. Data were fitted with a Boltzmann equation to estimate the $V_{1/2}$ for channel activation. Error bars indicate S.E.M

Table 2 Effects of $10\ \mu\text{M}$ **4e** on voltage dependence and kinetics of activation and deactivation on HCN1, HCN2, and HCN4 channels

Channel	$V_{1/2}$ (mV)		$\Delta V_{1/2}$ (mV)	τ_{act} (ms), $-120\ \text{mV}$		τ_{deact} (ms), $+50\ \text{mV}$	
	Control	$10\ \mu\text{M}$ 4e		Control	$10\ \mu\text{M}$ 4e	Control	$10\ \mu\text{M}$ 4e
HCN1	-73.8 ± 0.6	-107.8 ± 0.9	-30.4 ± 3.7	87.2 ± 7.5	$396.6 \pm 52.0^{***}$	22.8 ± 1.8	17.4 ± 2.4
HCN2	-89.9 ± 0.9	-120.7 ± 0.7	-30.2 ± 2.9	242.9 ± 24.0	$1598.0 \pm 154.4^{***}$	66.0 ± 4.2	75.6 ± 12.0
HCN4	-102.1 ± 0.9	-125.1 ± 2.2	-20.3 ± 3.4	855.7 ± 61.1	$2761.0 \pm 320.0^{***}$	92.9 ± 9.5	64.8 ± 5.9

*** $P < 0.001$ vs control

2% ($n = 4$) (Fig. 5b). The results indicated that **4e** was a non-use-dependent blocker of HCN channels.

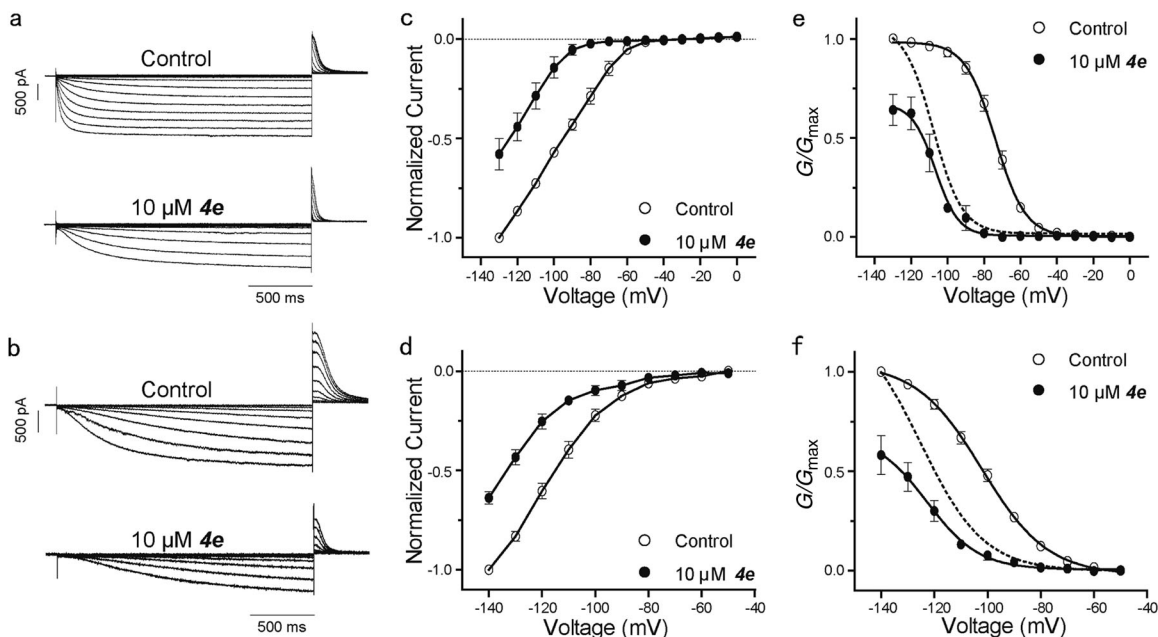
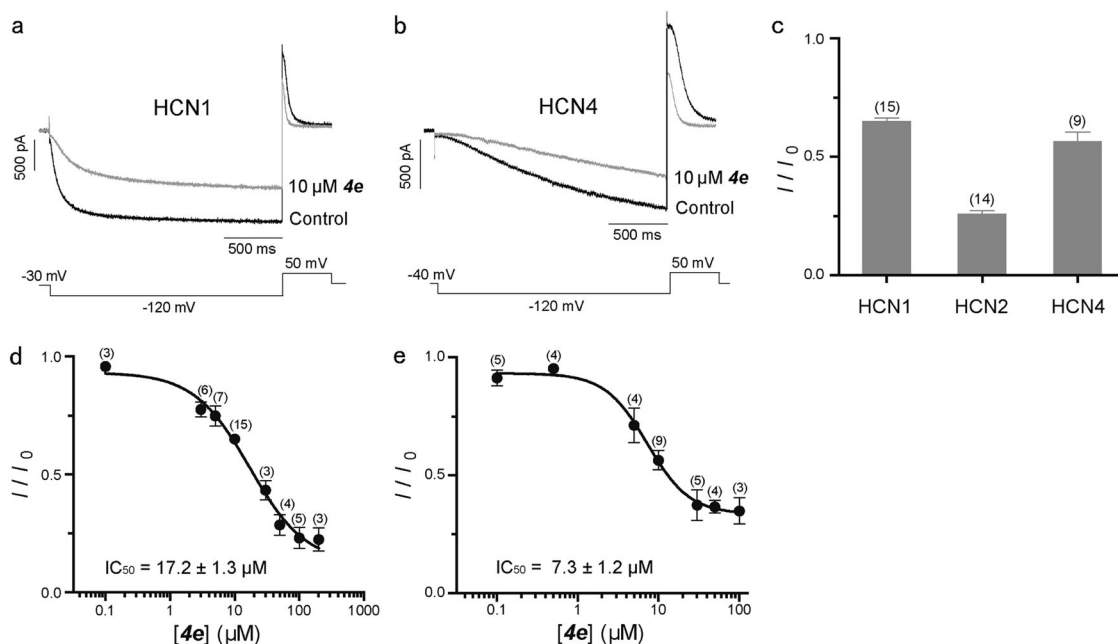
Influence of **4e** on I_h and action potential firing in small DRG neurons

As reported previously, HCN2 is the predominant HCN subunit that is expressed in small DRG neurons [32]. Cs^+ ($5\ \text{mM}$) and ZD7288 ($10\ \mu\text{M}$) were used as positive controls to confirm native I_h in the small DRG neurons in our study. The results show that I/I_0 is 0.04 ± 0.02 ($n = 4$) for Cs^+ and 0.51 ± 0.04 ($n = 7$) for ZD7288, respectively (Fig. 6a, b and d). The inhibitory properties of Cs^+ and ZD7288 were consistent with earlier studies [33–35]. Next, we examined whether $10\ \mu\text{M}$ **4e** could block native I_h in small DRG neurons. The results show that its I/I_0 is 0.28 ± 0.04 ($n = 13$) (Fig. 6c, d). Furthermore, we examined the influence of **4e** on the firing properties of small DRG neurons. As shown in Fig. 6e–g, the application of $10\ \mu\text{M}$ **4e** caused remarkably decreased action potential firing, which was induced by a $30\ \text{pA}$ current injection.

DISCUSSION

HCN channels play an important role in the heart and nervous system, in particular; HCN4 is expressed mostly in the heart and especially in the sinoatrial node, whereas the HCN1 and HCN2 channels are the predominant isoforms in neurons, and both contribute to spontaneous rhythm and firing frequency. Interestingly, it has been recently established that HCN channels are involved in autism spectrum disorder by interacting with Shank3 [36]. Therefore, HCN channels are an ideal new pharmacological targets for the treatment of disorders linked to abnormal excitability, such as inflammatory and neuropathic pain, epilepsy, arrhythmias, and tachycardia.

In the present study, we designed and synthesized novel alkanol amine compounds based on the compound **4a** and evaluated their ability to inhibit HCN channels (HCN1, 2, and 4). The most potent inhibitor in our study, **4e**, which was chemically distinct from previously reported HCN channel inhibitors, not only blocked HCN channel conductance but also dramatically left-



shifted their voltage-dependent activation, which indicates that it is a negative gating modifier other than a pure pore blocker. Compound **4e** blocked the HCN2 channel with an IC_{50} of 2.9 ± 1.2 μM at -120 mV and showed an inhibitory preference toward HCN2 compared with HCN1 or HCN4.

Previous studies have shown that ivabradine acts as a use-dependent blocker of HCN4 whose suppression effect only worked when the channel was in the "open state", and it acts as a non-open-dependent blocker of the HCN1 channel whose inhibition could only occur when channel was closed [26]. On the

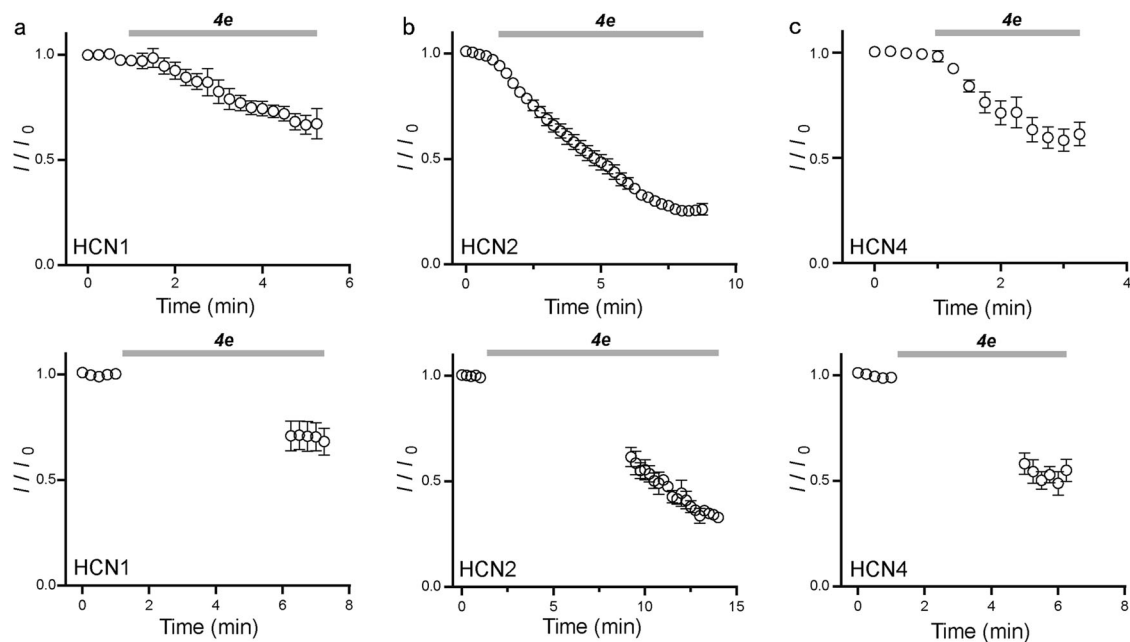


Fig. 5 The blockade of HCN channels by **4e** is non-use-dependent. **a–c** Upper: time course of the inhibition of HCN channels by 10 μM **4e** using the protocol shown in Fig. 3a (HCN1: $n = 7$, HCN2: $n = 8$, HCN4: $n = 5$). Below: Time course of the inhibition of HCN channels by 10 μM **4e** using a standard activation/deactivation protocol and HCN current was measured as shown before. At the beginning of the perfusion with 10 μM **4e**, the protocol was interrupted for several minutes (HCN1 was interrupted for 5 min, HCN2 for 8 min and HCN4 for 4 min), whereas the cell was held at the membrane voltage at -30 mV, then channel activation was resumed to test the use-dependence of **4e** (HCN1: $n = 4$, HCN2: $n = 4$, HCN4: $n = 4$)

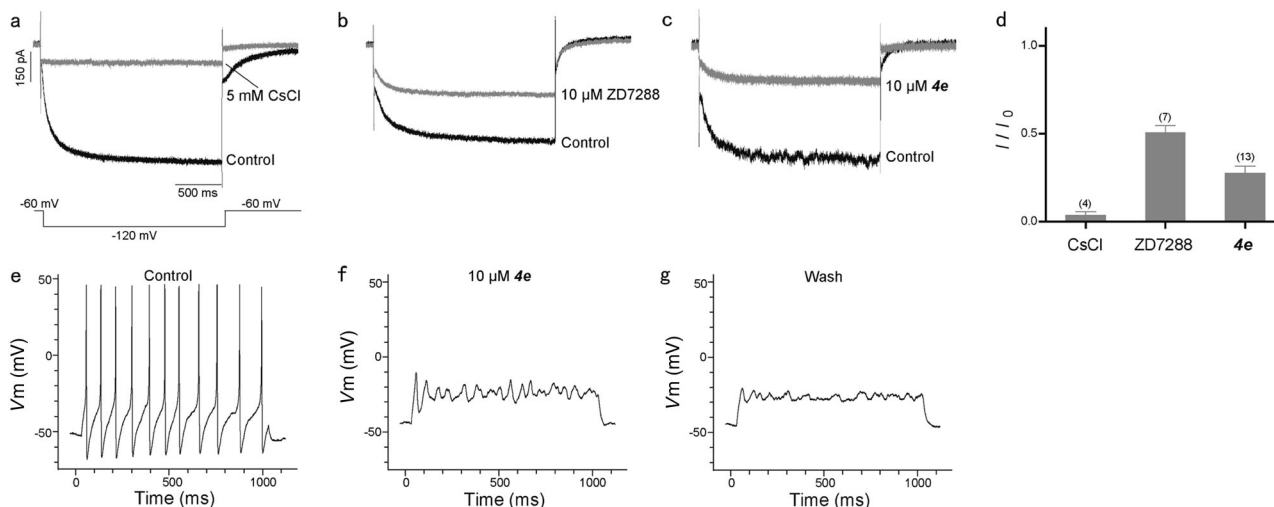


Fig. 6 The effect of **4e** in small DRG neurons. **a–c** Representative current traces of I_h measured with response to 5 mM CsCl **a**, 10 μM ZD7288 **b** and 10 μM **4e** **c**. The I_h current was elicited by a 2 s hyperpolarizing step at -120 mV from a holding potential of -60 mV. **d** Summary of inhibitory effect of 5 mM CsCl, 10 μM ZD7288, and 10 μM **4e** in small DRG neurons with a testing voltage of -120 mV. **e–f** Induced action potential firing of small DRG neurons was recorded under conditions without **e**, with **f** and wash **g** of 10 μM **4e**. A 1 s depolarization 30 pA current was injected into small DRG neurons to elicit the action potential through the recording electrode

other hand, ZD7288 is an obvious non-use-dependent blocker of the HCN1 channel [31]. In our study, we found that **4e** blocked HCN channels (HCN1, 2, and 4) both in the “closed state” and in the “open state” of channels, suggesting that **4e** was a non-use-dependent blocker of HCN channels.

DRG neurons are the first level of sensory afferent neurons, which are located in the peripheral nervous system, playing an indispensable role in the transmission of pain signals that transmit the information after painful injuries to the higher central nervous system. Therefore, new therapeutic strategies

that target DRG neurons in the peripheral nervous system to alleviate chronic pain have the advantage of minimizing side effects. Several ion channels (TRPA1, Nav1.7, and HCN channels) that are expressed in DRG neurons have been reported to play important roles in pain perception and transmission pathways [37]. Mouse DRG neurons were classified based on diameter of somata as follows: small ($< 20 \mu\text{m}$), medium ($20\text{--}30 \mu\text{m}$), and large ($> 30 \mu\text{m}$). HCN1 and HCN2 are predominantly expressed in DRG neurons and play a critical role in modulating firing frequency [38]. In particular, large DRG neurons mainly express

the HCN1 channel, which has faster activation kinetics and is less cAMP sensitive, and HCN1^{-/-} mice exhibited substantially less cold allodynia than wild-type littermates in a neuropathic pain model, suggesting an important role for HCN1 in neuropathic pain [38]. In the majority of small neurons, *I_h* has slower kinetics and is sensitive to intracellular cAMP, suggesting that it is mediated mainly by the HCN2 channel. Studies have shown that after knocking out the HCN2 channel in DRG neurons, thermal stimulation no longer caused hyperalgesia in inflammatory pain. Mechanical hyperalgesia, thermal hyperalgesia, and cold hyperalgesia were also significantly reduced in a neuropathic pain model. This study indicates that HCN2 plays an important role in both inflammatory pain and neuropathic pain in DRG neurons [39]. Furthermore, it was reported that ivabradine could suppress both the inflammatory and neuropathic pain by peripheral blockage of HCN channels [35]. Therefore, we tested the effect of **4e** on small DRG neurons to estimate the possibility of **4e** for the treatment of pain. The results showed that **4e** significantly reduced *I_h* in small DRG neurons and inhibited its action potential firing property.

Future animal behavior experiments are needed to investigate the possibility of the compound series for pain treatment identified in our study. In addition, **4e** provides a structural backbone for further modification, which would be valuable to identify more efficient and subtype-selective HCN channel inhibitors.

ACKNOWLEDGEMENTS

This work was supported by research grants from the National Natural Science Foundation of China 81503042 and Pearl River Nova Program of Guangzhou 201605111735229 (to PZ).

AUTHOR CONTRIBUTIONS

S-jC, YX and P-zZ designed the research; S-jC, Y-mL and YC performed the electrophysiological experiments; YX, J-yL and J-xP contributed new compounds; S-jC, YX and P-zZ analyzed the data and wrote the paper.

ADDITIONAL INFORMATION

The online version of this article (<https://doi.org/10.1038/s41401-018-0162-z>) contains supplementary material, which is available to authorized users.

Conflict of interest: The authors declare that they have no competing interest.

REFERENCES

- DiFrancesco D. Characterization of single pacemaker channels in cardiac sinoatrial node cells. *Nature*. 1986;324:470–3.
- Proenza C, Angoli D, Agranovich E, Macri V, Accili EA. Pacemaker channels produce an instantaneous current. *J Biol Chem*. 2002;277:5101–9.
- Baruscotti M, Bucchi A, DiFrancesco D. Physiology and pharmacology of the cardiac pacemaker (“funny”) current. *Pharmacol Ther*. 2005;107:59–79.
- Biel M, Wahl-Schott C, Michalakos S, Zong X. Hyperpolarization-activated cation channels: from genes to function. *Physiol Rev*. 2009;89:847–85.
- Sartiani L, Mannaioni G, Masi A, Novella Romanelli M, Cerbai E. The hyperpolarization-activated cyclic nucleotide-gated channels: from biophysics to pharmacology of a unique family of ion channels. *Pharmacol Rev*. 2017;69:354–95.
- DiFrancesco D, Tortora P. Direct activation of cardiac pacemaker channels by intracellular cyclic AMP. *Nature*. 1991;351:145–7.
- Gauss R, Seifert R, Kaupp UB. Molecular identification of a hyperpolarization-activated channel in sea urchin sperm. *Nature*. 1998;393:583–7.
- Wainger BJ, DeGennaro M, Santoro B, Siegelbaum SA, Tibbs GR. Molecular mechanism of cAMP modulation of HCN pacemaker channels. *Nature*. 2001;411:805–10.
- Craven KB, Zagotta WN. CNG and HCN channels: two peas, one pod. *Annu Rev Physiol*. 2006;68:375–401.
- Xu X, Vysotskaya ZV, Liu Q, Zhou L. Structural basis for the cAMP-dependent gating in the human HCN4 channel. *J Biol Chem*. 2010;285:37082–91.

- Ludwig A, Zong X, Stieber J, Hullin R, Hofmann F, Biel M. Two pacemaker channels from human heart with profoundly different activation kinetics. *EMBO J*. 1999;18:2323–9.
- Lorincz A, Notomi T, Tamas G, Shigemoto R, Nusser Z. Polarized and compartment-dependent distribution of HCN1 in pyramidal cell dendrites. *Nat Neurosci*. 2002;5:1185–93.
- Dobrzynski H, Boyett MR, Anderson RH. New insights into pacemaker activity: promoting understanding of sick sinus syndrome. *Circulation*. 2007;115:1921–32.
- Brioschi C, Micheloni S, Tellez JO, Pisoni G, Longhi R, Moroni P, et al. Distribution of the pacemaker HCN4 channel mRNA and protein in the rabbit sinoatrial node. *J Mol Cell Cardiol*. 2009;47:221–7.
- Schulze-Bahr E, Neu A, Friederich P, Kaupp UB, Breithardt G, Pongs O, et al. Pacemaker channel dysfunction in a patient with sinus node disease. *J Clin Invest*. 2003;111:1537–45.
- Baruscotti M, Bucchi A, Viscomi C, Mandelli G, Gonzalez G, Gneschi-Rusconi T, et al. Deep bradycardia and heart block caused by inducible cardiac-specific knockout of the pacemaker channel gene Hcn4. *Proc Natl Acad Sci U S A*. 2011;108:1705–10.
- Duhme N, Schweizer PA, Thomas D, Becker R, Schroter J, Barends TRM, et al. Altered HCN4 channel C-linker interaction is associated with familial tachycardia-bradycardia syndrome and atrial fibrillation. *Eur Heart J*. 2013;34:2768–75.
- Milano A, Vermeer AM, Lodder EM, Barc J, Verkerk AO, Postma AV, et al. HCN4 mutations in multiple families with bradycardia and left ventricular non-compaction cardiomyopathy. *J Am Coll Cardiol*. 2014;64:745–56.
- Nava C, Dalle C, Rastetter A, Striano P, de Kovel CG, Nabbout R, et al. De novo mutations in HCN1 cause early infantile epileptic encephalopathy. *Nat Genet*. 2014;46:640–5.
- Postea O, Biel M. Exploring HCN channels as novel drug targets. *Nat Rev Drug Discov*. 2011;10:903–14.
- Thollon C, Cambarrat C, Vian J, Prost JF, Peglion JL, Vilaine JP. Electrophysiological effects of S 16257, a novel sino-atrial node modulator, on rabbit and guinea-pig cardiac preparations: comparison with UL-FS 49. *Br J Pharmacol*. 1994;112:37–42.
- Bois P, Bescond J, Renaudon B, Lenfant J. Mode of action of bradycardic agent, S 16257, on ionic currents of rabbit sinoatrial node cells. *Br J Pharmacol*. 1996;118:1051–7.
- BoSmith RE, Briggs I, Sturgess NC. Inhibitory actions of ZENECA ZD7288 on whole-cell hyperpolarization activated inward current (I_f) in guinea-pig dissociated sinoatrial node cells. *Br J Pharmacol*. 1993;110:343–9.
- Cheng L, Kinarid K, Rajamani R, Sanguinetti MC. Molecular mapping of the binding site for a blocker of hyperpolarization-activated, cyclic nucleotide-modulated pacemaker channels. *J Pharmacol Exp Ther*. 2007;322:931–9.
- Shin KS, Rothberg BS, Yellen G. Blocker state dependence and trapping in hyperpolarization-activated cation channels: evidence for an intracellular activation gate. *J Gen Physiol*. 2001;117:91–101.
- Bucchi A, Tognati A, Milanese R, Baruscotti M, DiFrancesco D. Properties of ivabradine-induced block of HCN1 and HCN4 pacemaker channels. *J Physiol*. 2006;572:335–46.
- Bucchi A, Baruscotti M, Nardini M, Barbuti A, Micheloni S, Bolognesi M, et al. Identification of the molecular site of ivabradine binding to HCN4 channels. *PLoS One*. 2013;8:e53132.
- Melchiorre M, Del Lungo M, Guandalini L, Martini E, Dei S, Manetti D, et al. Design, synthesis, and preliminary biological evaluation of new isoform-selective f-current blockers. *J Med Chem*. 2010;53:6773–7.
- Del Lungo M, Melchiorre M, Guandalini L, Sartiani L, Mugelli A, Koncz I, et al. Novel blockers of hyperpolarization-activated current with isoform selectivity in recombinant cells and native tissue. *Br J Pharmacol*. 2012;166:602–16.
- Stieber J, Wieland K, Stockl G, Ludwig A, Hofmann F. Bradycardic and proarrhythmic properties of sinus node inhibitors. *Mol Pharmacol*. 2006;69:1328–37.
- Gill CH, Randall A, Bates SA, Hill K, Owen D, Larkman PM, et al. Characterization of the human HCN1 channel and its inhibition by capsazepine. *Br J Pharmacol*. 2004;143:411–21.
- Schnorr S, Eberhardt M, Kistner K, Rajab H, Kasser J, Hess A, et al. HCN2 channels account for mechanical (but not heat) hyperalgesia during long-standing inflammation. *Pain*. 2014;155:1079–90.
- Bischoff U, Brau ME, Vogel W, Hempelmann G, Olschewski A. Local anaesthetics block hyperpolarization-activated inward current in rat small dorsal root ganglion neurones. *Br J Pharmacol*. 2003;139:1273–80.
- Yao H, Donnelly DF, Ma C, LaMotte RH. Upregulation of the hyperpolarization-activated cation current after chronic compression of the dorsal root ganglion. *J Neurosci*. 2003;23:2069–74.
- Young GT, Emery EC, Mooney ER, Tsantoulas C, McNaughton PA. Inflammatory and neuropathic pain are rapidly suppressed by peripheral block of hyperpolarisation-activated cyclic nucleotide-gated ion channels. *Pain*. 2014;155:1708–19.

36. Yi F, Danko T, Botelho SC, Patzke C, Pak C, Wernig M, et al. Autism-associated SHANK3 haploinsufficiency causes I_h channelopathy in human neurons. *Science*. 2016;352:aaf2669.
37. Berta T, Qadri Y, Tan PH, Ji RR. Targeting dorsal root ganglia and primary sensory neurons for the treatment of chronic pain. *Expert Opin Ther Targets*. 2017;21:695–703.
38. Momin A, Cadiou H, Mason A, McNaughton PA. Role of the hyperpolarization-activated current I_h in somatosensory neurons. *J Physiol*. 2008;586: 5911–29.
39. Emery EC, Young GT, Berrocoso EM, Chen L, McNaughton PA. HCN2 ion channels play a central role in inflammatory and neuropathic pain. *Science*. 2011;333: 1462–6.